Improving the performance of Perfectly Matched Layers by means of hp-adaptivity

C. Michler*, L. Demkowicz, J. Kurtz and D. Pardo
Institute for Computational Engineering and Sciences (ICES)
The University of Texas at Austin
201 East 24th Street, ACES Building
Austin, Texas 78712, U.S.A.
E-mail: c.michler@ices.utexas.edu

ABSTRACT

We improve the performance of the Perfectly Matched Layer by using an automatic hp-adaptive discretization. By means of hp-adaptivity, we obtain a sequence of discrete solutions that converges exponentially to the continuum solution. Asymptotically, we thus recover the property of the PML of having a zero reflection coefficient for all angles of incidence and all frequencies on the continuum level. This allows us to minimize the reflections from the discrete PML to an arbitrary level of accuracy while retaining optimal computational efficiency. Since our hp-adaptive scheme is automatic, no interaction with the user is required. This renders tedious parameter tuning of the PML obsolete. We demonstrate the improvement of the PML performance by hp-adaptivity through numerical results for acoustic, elastodynamic and electromagnetic wave-propagation problems in the frequency domain and in different systems of coordinates.

Keywords and Phrases: Perfectly Matched Layer, hp-adaptivity, exterior boundary-value problem, acoustic scattering, elastodynamic wave propagation, electromagnetic scattering.

1. Introduction

Most wave-propagation problems arising in acoustics, elastodynamics and electromagnetics are posed on a spatially unbounded domain. Since domain-based discretization methods such as finite elements can handle only bounded domains, a truncation of the unbounded physical domain to a bounded computational domain is necessary. Any artificial boundary condition that is applied on the truncated domain boundary must not essentially alter the original problem, i.e. it must allow for outgoing waves only and it has to be essentially reflectionless. Many techniques have been developed for this purpose such as Infinite Elements (see e.g. [4, 12]), the Dirichlet-to-Neumann map (see e.g. [14]), exact nonreflecting boundary conditions (see e.g. [15]), the continued-fraction absorbing boundary condition [16] and the Perfectly Matched Layer [3]. We refer to Refs. [17, 26, 31] for an overview over these so-called *absorbing boundary conditions*, all of which have their specific strengths and weaknesses.

Among the various absorbing boundary conditions, the Perfectly Matched Layer (PML) in particular has become very popular due to its performance, conceptual simplicity and ease of implementation. The PML is based on the concept of analytic continuation of a real function into the complex plane (see e.g. [13]), typically also referred to as *complex-coordinate stretching* [8]. This concept enables straightforward derivation of the PML equations for different types of wave propagation and different systems of coordinates; see e.g. Refs. [24, 25, 30, 32]. The PML concept has been extensively studied and analyzed regarding the so-called split and unsplit formulations and well-posedness (see e.g. Refs. [1, 19]), causality [6, 29], long-time behavior [1, 2], termination of the PML [9, 27] and finite-element dispersion and convergence analysis in the frequency domain [5, 18]. A recommendable review of the PML in the context of Maxwell's equations is presented in Ref. [30].

The PML has the remarkable property of having a zero reflection coefficient for all angles of incidence and all frequencies on the continuum level. However, under discretization, this property is

compromised and spurious reflections typically do occur at the discrete PML. Much effort has thus been spent on optimizing the PML parameters to minimize the error resulting from discretization and thus obtain optimal performance of the PML; see e.g. [7, 9, 28]. In this work, we advocate the opposite approach, i.e. we optimize the discretization for any given PML parameters, rather than resorting to tedious parameter tuning. A highly effective methodology to construct an optimal discretization is the *hp*-adaptive finite-element method that allows for locally adapting the element size h and polynomial approximation order p to the local resolution requirements of the solution. Such adaptivity can be accomplished in an automatic way, i.e. no interaction with the user is required. This is achieved by a so-called two-grid strategy [10] that guides the adaptive refinements. By solving the problem on a sequence of coarse and corresponding fine grids, an approximation of the error function is constructed at each iteration, which serves as an error estimate and based on which it is determined where to refine and how to refine, i.e. in h or in p. This yields optimal accuracy for the least computational expense. For details on the automatic *hp*-adaptive procedure, we refer to Ref. [10] and to the recent book by Demkowicz [11]. The immense benefit that *hp*-adaptivity can offer for increasing the performance of the PML is due to the property of the PML of having a zero reflection coefficient on the continuum level. Although this property is lost under discretization, it can be recovered asymptotically, i.e. upon convergence to the continuum solution. This implies that upon convergence of the *hp*-adaptive discretization, the discretization error and the resulting reflections can be minimized to an arbitrary level of accuracy.

The PML is designed such that traveling waves that leave the actual domain of interest and enter the encompassing PML are converted into evanescent waves that are made to decay sufficiently fast, i.e. they vanish before they can get reflected at the domain boundary. The rapid decay that is enforced on the solution in the PML implies strong solution gradients which need to be resolved to prevent reflections and an accompanying loss in accuracy. Although the significance of resolving the PML has long been recognized, conventional discretization methods generally face difficulties in resolving strong solution gradients and, therefore, typically revert to adjusting the PML parameters and the associated damping profile to a given discretization. Conversely, our adaptive strategy automatically adapts the discretization to resolve any damping profile that is imposed on the solution. This allows us to choose the geometry of the PML independent of the geometry of the initial grid, i.e. the respective geometries need not coincide (a cylindrical PML and a Cartesian grid, for instance) - a truly remarkable feature. In this paper, we show that by means of *hp*-adaptivity PML-induced solution gradients can be effectively resolved and the performance of the PML can be greatly improved. This renders tedious parameter tuning of the PML obsolete. We demonstrate the performance and the versatility of our approach by numerical results for acoustic, elastodynamic and electromagnetic wave-propagation problems in the frequency domain and in different systems of coordinates.

The contents of this paper are organized as follows: Sections 2, 3 and 4 present the PML formulation of the Helmholtz, linear elasticity and Maxwell's equations, respectively, and discuss the particularities of the respective PML formulation. Each of these sections presents numerical results that demonstrate the potential of *hp*-adaptivity for improving the performance of the PML. Finally, Section 5 contains concluding remarks.

2. Helmholtz equation

In this section, we study the formulation of the Perfectly Matched Layer for an exterior boundary-value problem governed by the Helmholtz equation. In Section 2.1, we provide a problem statement in coordinate-invariant form. In Section 2.2, we derive the PML formulation in Cartesian coordinates. Based on the formalism introduced in Section 2.2, in Sections 2.3 and 2.4, we state the PML formulation in 2D polar and 3D spherical coordinates, respectively. In Section 2.5, we present numerical results for exterior Helmholtz problems that demonstrate the improvement in performance of the PML that can be obtained by *hp*-adaptive finite elements.

2.1 The Helmholtz equation in coordinate-invariant form

We consider the unbounded exterior domain $\Omega = \mathbb{R}^n - \Omega^{\text{int}}$ with $\Omega^{\text{int}} \subset \mathbb{R}^n$, $n = 1, 2, 3$, a given bounded interior domain and n the number of space dimensions. We seek a solution for the pressure $p(\boldsymbol{x})$, $\boldsymbol{x} \in \bar{\Omega}$ that satisfies the Helmholtz equation in Ω,

$$-\Delta p - k^2 p = 0 \quad \text{in}\, \Omega\,, \tag{2.1}$$

where Δ denotes the Laplacian operator, and $k := \omega/c$ is the wavenumber with ω and c the angular frequency and the sound speed, respectively. Throughout this work, we shall assume a time-harmonic dependence of the form $e^{i\omega t}$, where i is the imaginary unit and t denotes time and, moreover, we consider the governing equations in their non-dimensional form. Eq. (2.1) is supplemented with a Dirichlet boundary condition on the interior-domain boundary

$$p = p_D \quad \text{on}\, \Gamma = \partial\Omega^{\text{int}}\,, \tag{2.2}$$

and the Sommerfeld radiation condition at infinity

$$\frac{\partial p}{\partial r} + ikp \in L^2(\Omega)\,, \tag{2.3}$$

where r denotes the radius. Note that this particular form of the Sommerfeld radiation condition has the advantage of being independent of the number of space dimensions. We further remark that the Dirichlet boundary condition (2.2) can be replaced by a Neumann or a Cauchy (impedance) boundary condition,

$$\frac{\partial p}{\partial \boldsymbol{n}} = g\,, \tag{2.4a}$$

$$\frac{\partial p}{\partial \boldsymbol{n}} + i\omega\beta p = g\,, \tag{2.4b}$$

on the entire boundary or on parts of it, where $\boldsymbol{n}$ denotes the outward unit normal on Γ, and $\beta > 0$ and g are given functions on Γ.

Finally, let us remark that the Helmholtz equation is obtained by eliminating the velocity from the first-order system of linear acoustics equations which, in coordinate-invariant form, are

$$\begin{cases} i\omega p + \rho_0 c^2 \boldsymbol{\nabla} \cdot \boldsymbol{u} &= 0 \\ i\omega \rho_0 \boldsymbol{u} + \boldsymbol{\nabla} p &= \boldsymbol{0}\,, \end{cases} \tag{2.5}$$

where p and $\boldsymbol{u}$ denote the small-amplitude disturbance in pressure and velocity, respectively, of a uniform stationary fluid, and ρ_0 is the fluid density associated with this uniform state.

2.2 PML formulation of the Helmholtz equation in Cartesian coordinates

The governing equations in the PML can be derived by applying a complex coordinate transformation of the original equations in the direction normal to the interface between the "domain of interest" and the PML. For this purpose, it is essential that the solution to the considered equations is analytic in the direction normal to the interface. Analyticity of the solution is equivalent to the solution being holomorphic, i.e. differentiable in the complex sense. This assumption allows us to consider the solution as a function of complex variables z_i in place of real variables x_i, and to replace the derivative with respect to x_i with the derivative with respect to z_i. This procedure is commonly also referred to as *analytic continuation* [13] or as *complex-coordinate stretching* [8]. The motivation of such coordinate stretching is to construct a continuation of the solution into the complex plane in such a way that, in the PML, the solution becomes evanescent, whereas in the domain of interest the original solution is retained.

The analytic continuation of the solution into the complex plane is obtained by the following transformation of the j-th coordinate

$$x_j \to z_j(x_j) := [x_j + a_j(x_j)] - i[b_j(x_j)] \qquad j = 1, \ldots, n\,, \tag{2.6a}$$

$$\frac{\partial}{\partial x_j} \to \frac{\partial}{\partial z_j(x_j)} = \frac{1}{z_j'}\frac{\partial}{\partial x_j} \quad \text{with} \quad z_j' := \frac{dz_j(x_j)}{dx_j} = \left[1 + \frac{da_j(x_j)}{dx_j}\right] - i\left[\frac{db_j(x_j)}{dx_j}\right], \tag{2.6b}$$

where the j-th complex coordinate z_j depends only on the j-th real coordinate x_j. Factors $a_j(x_j)$ and $b_j(x_j)$ are "suitable" functions specified in the sequel. In the domain of interest, $a_j(x_j) = b_j(x_j) = 0$ which yields $z_j(x_j) = x_j$ and, thus, the original, "unstretched" equations are recovered. A jump in a_j, b_j across the interface between the domain of interest and the PML induces a loss of regularity. To minimize such loss of regularity, $a_j(x_j)$ and $b_j(x_j)$ are typically set to increase steadily from zero as one moves away from the interface through the PML, ideally with C^K-continuity across the interface. Considering a wave traveling to the right, in the PML, $a_j(x_j) \geq 0$ to ensure that evanescent waves have an exponential decay that is faster in the PML than in the domain of interest; and $b_j(x_j) \geq 0$ to ensure that traveling waves, once they enter the PML, are converted into evanescent waves that decay exponentially. Conversely, for a wave traveling to the left, we need $a_j(x_j) \leq 0$ and $b_j(x_j) \leq 0$ in the PML. We remark that, in general, $b_j(x_j)$ is chosen frequency-dependent; see for instance Ref. [30]. However, in this work, we shall not consider frequency-dependent stretching, since all our examples consider a single frequency only. By an appropriate choice of $a_j(x_j)$ and $b_j(x_j)$, a sufficiently fast decay of the solution can be enforced such that the solution of the PML-modified problem practically vanishes at the truncated domain boundary and, thus, satisfies a homogeneous Dirichlet boundary condition. Note, however, that the enforced rapid decay of the solution in the PML induces strong solution gradients. We demonstrate in Section 2.5 the importance of resolving these PML-induced solution gradients for the accuracy of the solution in the domain of interest and, moreover, that this can be efficiently achieved by *hp*-adaptivity. Finally, let us remark that the choice of $a_j(x_j)$ and $b_j(x_j)$ has to respect the principle of causality; see Refs. [6, 29] for details.

In the sequel, we derive the PML formulation for the Helmholtz problem considered in Section 2.1 in n dimensions and Cartesian coordinates. To this end, we start from the time-harmonic linear acoustics equations (2.5) expressed in Cartesian coordinates

$$\begin{cases} i\omega p + \rho_0 c^2 \displaystyle\sum_{j=1}^{n} \frac{\partial u_j}{\partial x_j} &= 0\,, \\ i\omega \rho_0 u_j + \dfrac{\partial p}{\partial x_j} &= 0\,. \end{cases} \tag{2.7}$$

Introducing in Eqs. (2.7) complex-coordinate stretching according to (2.6) with $x_j \to z_j(x_j)$, we obtain

$$\begin{cases} i\omega p + \rho_0 c^2 \displaystyle\sum_{j=1}^{n} \frac{1}{z_j'}\frac{\partial u_j}{\partial x_j} &= 0\,, \\ i\omega \rho_0 u_j + \dfrac{1}{z_j'}\dfrac{\partial p}{\partial x_j} &= 0\,. \end{cases} \tag{2.8}$$

Note that we do not use the Einstein summation convention here. To express Eq. $(2.8)_1$ in a weak form, we multiply $(2.8)_1$ with $z' := \Pi_{j=1}^{n} z_j'$, and then with a test function $q \in \mathcal{Q}$ and integrate over the domain Ω. Thus, we obtain

$$i\omega \int_\Omega z' p q \, d\Omega + \rho_0 c^2 \sum_{j=1}^{n} \int_\Omega \frac{z'}{z_j'}\frac{\partial u_j}{\partial x_j} q \, d\Omega = 0\,. \tag{2.9}$$

Note that in deriving the weak form (2.9) the multiplication of the expression by z' facilitates the subsequent integration-by-parts, because the prefactor z'/z_j' in (2.9) is independent of x_j. Upon

integrating Eq. (2.9) by parts, we multiply the resulting expression by $i\omega$ and eliminate u_j by invoking Eq. $(2.8)_2$. This yields the final variational form

$$\begin{cases} p \in \hat{p}_D + \mathcal{Q} \\ -k^2 \int_\Omega z' p q \, d\Omega + \sum_{j=1}^{n} \int_\Omega \frac{z'}{(z'_j)^2} \frac{\partial p}{\partial x_j} \frac{\partial q}{\partial x_j} \, d\Omega = \int_{\Gamma_N} g q \, dS \\ \qquad\qquad\qquad\qquad\qquad\qquad\qquad\qquad \forall q \in \mathcal{Q} \,, \end{cases} \tag{2.10}$$

where $k = \omega/c$ is the wavenumber and g denotes the normal pressure gradient specified on the Neumann portion of the boundary, Γ_N. In (2.10), $\hat{p}_D$ denotes a finite-energy lift of the Dirichlet data, $\mathcal{Q}$ is the space of test functions

$$\mathcal{Q} := \{ q \in \mathcal{X} \, : \, q = 0 \text{ on } \Gamma_D \} \,, \tag{2.11}$$

and the "energy space" $\mathcal{X}$ associated with the variational problem (2.10) is defined as

$$\mathcal{X} := \left\{ q \, : \, |z'|^{\frac{1}{2}} \, q, \left| \frac{z'}{(z'_j)^2} \right|^{\frac{1}{2}} \frac{\partial q}{\partial x_j} \in L^2(\Omega) \right\} . \tag{2.12}$$

Note that in deriving Eq. (2.10), Eq. $(2.7)_1$ has been treated in its weak form, whereas Eq. $(2.7)_2$ has been treated in its strong form. This has implications for the regularity requirements of the solution variables. In particular, this relaxes the regularity requirements for the velocity u_j.

Finally, let us remark that, since the complex-coordinate stretching according to (2.6) is straightforward for first-order derivatives, the variational formulation of the PML equations is most conveniently derived by starting from a system of first-order equations and following the procedure described above. This equally applies to the PML formulation of the linear elasticity equations as well as to the PML formulation of Maxwell's equations that are stated in Sections 3.1 and 4.1, respectively.

2.3 PML formulation of the Helmholtz equation in 2D polar coordinates

In this section, we present the PML formulation for the Helmholtz equation in two dimensions and polar coordinates (r, θ) with $x = r\cos\theta$ and $y = r\sin\theta$. We employ complex-coordinate stretching only in the r coordinate, i.e. normal to the interface between the domain of interest and the PML. Thus, the solution to the Helmholtz equation is required to be analytic in the r coordinate only, but not necessarily in the θ coordinate.

Since the derivation of the PML formulation for polar coordinates proceeds analogously to the case of Cartesian coordinates (cf. Section 2.2), let us defer the derivation to Appendix A and state here only the final variational formulation with complex-coordinate stretching according to (2.6) with $r \to z(r)$

$$\begin{cases} p \in \hat{p}_D + \mathcal{Q} \\ \int_\Omega \left(\frac{z}{z'r} \frac{\partial p}{\partial r} \frac{\partial q}{\partial r} + \frac{z'}{rz} \frac{\partial p}{\partial \theta} \frac{\partial q}{\partial \theta} \right) r dr d\theta - k^2 \int_\Omega \frac{z'z}{r} p q \, r dr d\theta = 0 \\ \qquad\qquad\qquad\qquad\qquad\qquad\qquad\qquad \forall q \in \mathcal{Q} \,. \end{cases} \tag{2.13}$$

In (2.13), $\hat{p}_D$ denotes a finite-energy lift of the Dirichlet data, $\mathcal{Q}$ is the space of test functions

$$\mathcal{Q} := \{ q \in \mathcal{X} \, : \, q = 0 \text{ on } \Gamma \} \,, \tag{2.14}$$

where we tacitly assumed Dirichlet boundary conditions for the solution on the entire boundary, Γ, and, accordingly, homogeneous boundary conditions for the test function q, and the "energy space" $\mathcal{X}$ associated with the variational problem (2.13) is defined as

$$\mathcal{X} := \left\{ q \, : \, \left| \frac{z'z}{r} \right|^{\frac{1}{2}} q, \left| \frac{z}{z'r} \right|^{\frac{1}{2}} \frac{\partial q}{\partial r}, \left| \frac{z'}{rz} \right|^{\frac{1}{2}} \frac{\partial q}{\partial \theta} \in L^2(\Omega) \right\} . \tag{2.15}$$

Since the solution to problem (2.13) decays exponentially in r, we replace, upon discretization, the infinite physical domain by a finite computational domain. We can then discretize problem (2.13) on the truncated domain by means of finite elements. Note that the truncated domain need not have a circular shape; moreover, we typically revert to Cartesian coordinates x_j to represent the integrand of Eq. (2.13). In particular, the integrand of the first integral in (2.13) can then be rewritten as

$$\begin{aligned}\frac{z}{z'r}\frac{\partial p}{\partial r}\frac{\partial q}{\partial r}+\frac{z'}{rz}\frac{\partial p}{\partial \theta}\frac{\partial q}{\partial \theta} &= \frac{z}{z'r}\frac{\partial p}{\partial r}\frac{\partial q}{\partial r}+\frac{z'r}{z}\left(\frac{\partial p}{\partial x_j}\frac{\partial q}{\partial x_j}-\frac{\partial p}{\partial r}\frac{\partial q}{\partial r}\right)\\ &= \frac{z'r}{z}\frac{\partial p}{\partial x_j}\frac{\partial q}{\partial x_j}+\left(\frac{z}{z'r}-\frac{z'r}{z}\right)\frac{\partial p}{\partial r}\frac{\partial q}{\partial r}\\ &= a_{ij}\frac{\partial p}{\partial x_j}\frac{\partial q}{\partial x_i}\end{aligned} \tag{2.16a}$$

with

$$a_{ij}=\frac{z'r}{z}\delta_{ij}+\left(\frac{z}{z'r}-\frac{z'r}{z}\right)\frac{x_i x_j}{r^2}\,, \tag{2.16b}$$

where δ_{ij} denotes the Kronecker delta and the Einstein summation convention has been used. The first equality in (2.16a) is obtained by invoking Eq. (A.58a), and the third equality is obtained by using the fact that

$$\frac{\partial p}{\partial r}=\frac{\partial p}{\partial x_j}\frac{\partial x_j}{\partial r}=\frac{\partial p}{\partial x_j}\frac{x_j}{r}\,, \tag{2.17}$$

and likewise for $\partial q/\partial r$.

2.4 PML formulation of the Helmholtz equation in 3D spherical coordinates

In this section, we present the PML formulation for the Helmholtz equation in three dimensions and standard spherical coordinates (r,ψ,θ) with $x=r\sin\psi\cos\theta$, $y=r\sin\psi\sin\theta$ and $z=r\cos\psi$. Since the derivation proceeds analogously to the case of Cartesian coordinates (cf. Section 2.2), let us defer the derivation to Appendix B and state here only the final variational formulation with complex-coordinate stretching according to (2.6) with $r\to z(r)$

$$\left\{\begin{array}{l} p\in\hat{p}_D+\mathcal{Q}\\ \displaystyle\int_\Omega\left(\frac{z^2}{z'r^2}\frac{\partial p}{\partial r}\frac{\partial q}{\partial r}+\frac{z'}{r^2}\frac{\partial p}{\partial \psi}\frac{\partial q}{\partial \psi}+\frac{z'}{r^2\sin^2\psi}\frac{\partial p}{\partial \theta}\frac{\partial q}{\partial \theta}-k^2z'\frac{z^2}{r^2}pq\right)r^2\sin\psi drd\psi d\theta=\int_{\Gamma_N}gq\,dS\\ \hfill\forall q\in\mathcal{Q}\,,\end{array}\right. \tag{2.18}$$

where g denotes the normal pressure gradient specified on the Neumann portion of the boundary, Γ_N. For the remainder of the boundary, Γ_D, we assume Dirichlet boundary conditions for the pressure and, accordingly, homogeneous boundary conditions for the test function q. In (2.18), $\hat{p}_D$ denotes a finite-energy lift of the Dirichlet data, $\mathcal{Q}$ is the space of test functions

$$\mathcal{Q}:=\{q\in\mathcal{X}\;:\;q=0\text{ on }\Gamma_D\}\,, \tag{2.19}$$

and the "energy space" $\mathcal{X}$ is defined as

$$\mathcal{X}:=\left\{q\;:\;\frac{|z'|^{\frac12}|z|}{r}q\in L^2(\Omega),\;\frac{|z|}{|z'|^{\frac12}r}\frac{\partial q}{\partial r}\in L^2(\Omega),\;\frac{|z'|^{\frac12}}{r}\boldsymbol{\nabla}_{\mathrm{s}}\,q\in\boldsymbol{L}^2(\Omega)\right\}\,, \tag{2.20}$$

where $\boldsymbol{\nabla}_{\mathrm{s}}$ denotes the gradient on the unit sphere

$$\boldsymbol{\nabla}_{\mathrm{s}}\,q=\frac{1}{\sin\psi}\frac{\partial q}{\partial \theta}\boldsymbol{e}_\theta+\frac{\partial q}{\partial \psi}\boldsymbol{e}_\psi\,. \tag{2.21}$$

2.5 Numerical experiments

To demonstrate the benefit of *hp*-adaptivity for the performance of the PML, we present below numerical results of wave propagation in an acoustic medium. In particular, we consider the scattering of a 2D plane wave on a cylinder with a polar PML and, subsequently, the scattering of a 3D plane wave on a sphere with spherical PML.

2D polar PML

In this section, we test the *hp*-adaptive algorithm for a two-dimensional PML in polar coordinates for the time-harmonic linear acoustics equations according to Eq. (2.13). This problem is suitable for assessing the performance of the PML combined with *hp*-adaptivity and the accuracy of the numerical solution, since the problem admits an analytic solution (see e.g. [21, ch. 10.5]), which is expressed in terms of standard harmonics and Hankel functions. The validity of the analytic solution is extended to the PML by means of complex-coordinate stretching. Note that the computational domain need not have a cylindrical shape. In fact, to challenge our *hp*-adaptive algorithm, we select a cylindrical geometry of the PML that does not match the Cartesian structure of the initial mesh. Thus, we "truncate" the Cartesian computational domain $(-5,5)^2$ by a cylindrical PML for $r \geq 4$. Complex-coordinate stretching is invoked in the r coordinate only, in particular

$$z(r) = \begin{cases} r & 0 \leq r < 4 \\ r - i\left(\frac{r-4}{0.5}\right)^5 r & r \geq 4 \end{cases} . \tag{2.22}$$

Let us however remark that the stretching (2.22) is just one possible choice that ensures a sufficiently rapid decay of the solution and that other forms are conceivable.

Below, we present numerical results for the scattering of an incident plane wave $p^{\text{inc}} = e^{-ik\boldsymbol{v}\cdot\boldsymbol{x}}$ on a cylinder. We set the dimensionless cylinder radius $r = 1$, the dimensionless wavenumber $k = 4\pi/3$ and the direction of the incident wave $\boldsymbol{v} = (1, 0)$. We augment the problem with homogeneous Dirichlet boundary conditions $p = 0$ on the outer domain boundary adjacent to the PML and, moreover, with Dirichlet boundary conditions on the cylinder boundary, i.e. at $r = 1$, that are specified according to the analytic solution from Ref. [21, ch. 10.5].

Starting from the initial mesh shown in Fig. 1 *(left)*, we plot in Fig. 4 *(right)* the convergence curve in terms of percent relative error in the H^1-seminorm (in a logarithmic scale) versus the total number of degrees-of-freedom N (in the algebraic scale $N^{1/3}$). The error is evaluated over the entire computational domain including the PML. Fig. 4 *(right)* displays two convergence curves for the cylindrical PML that use as a reference solution the exact analytic solution and the fine-grid solution, respectively. These two convergence curves are almost indistinguishable, which indicates that the error estimate obtained with the fine-grid solution as reference solution is indeed very accurate. The *hp*-refined mesh corresponding to an error level of 1% is obtained after 16 iterations; see Fig. 1 *(right)*. Note the refinements that have been selected by the adaptive algorithm in particular in the PML to resolve the cylindrical geometry of the PML and the solution that is made to decay rapidly in radial direction in the PML. Figs. 2 *(left)* and *(right)* show the real component of the solution and of the error function, respectively. Here, the error function is computed using the analytic solution to the problem; cf. [21]. These plots demonstrate that *hp*-adaptivity is capable of effectively resolving the rapidly decaying solution in the PML, thereby minimizing the reflections from the PML to an arbitrary level of accuracy (here 1%) without the necessity of PML-parameter tuning. These results are truly remarkable given the mismatch between the cylindrical PML and the Cartesian structure of the initial mesh.

Clearly, if the geometry of the PML is chosen according to the structure of the underlying mesh, significantly fewer degrees-of-freedom are required to deliver the same accuracy. To support this claim, we recompute the above test case with a Cartesian PML specified according to

$$z_k(x_k) = \begin{cases} x_k & 0 \leq |x_k| < 4 \\ x_k - i\left(\frac{|x_k|-4}{0.5}\right)^5 x_k & |x_k| \geq 4 \end{cases} \qquad k = 1, 2\,. \tag{2.23}$$

Starting from the same initial mesh as displayed in Fig. 1 *(left)*, an *hp*-mesh corresponding to an error level of 1% is obtained after 15 iterations; see Fig. 3 *(left)* for the *hp*-refined mesh, Fig. 4 *(left)* for the real component of the error function with the fine-grid solution used as a reference, and Fig. 4 *(right)* for the convergence curve. The real component of the solution obtained on the *hp*-refined mesh is shown in Fig. 3 *(right)*. Comparing the final *hp*-meshes for a cylindrical and a Cartesian PML, Fig. 1 *(right)* and Fig. 3 *(left)*, respectively, we observe that the *hp*-mesh for a cylindrical PML consists of 8325 degrees-of-freedom, whereas the *hp*-mesh for a Cartesian PML consists only of 4779 degrees-of-freedom; compare also the respective convergence curves in Fig. 4 *(right)*. Hence, the efficiency of the discretization can be significantly improved by constructing initial meshes in accordance with the geometry of the PML.

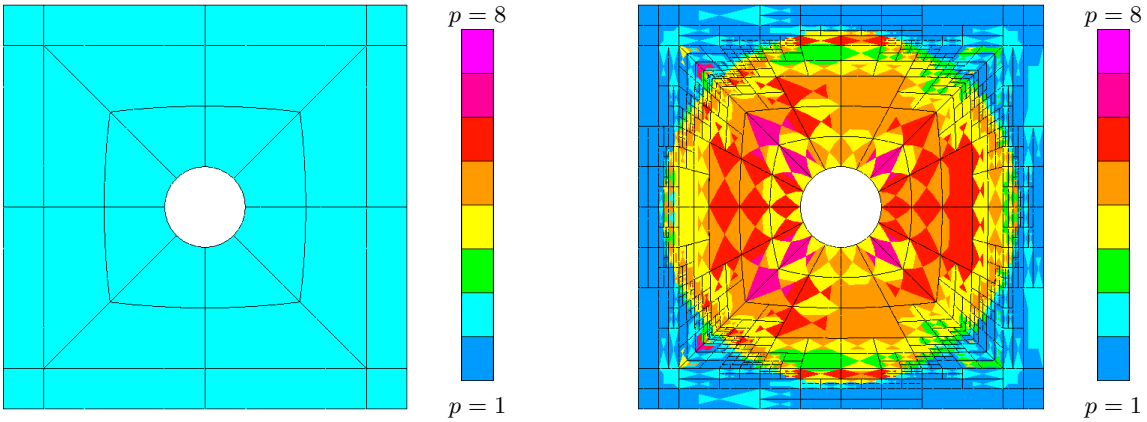

Figure 1: Acoustic scattering of a plane wave on a unit cylinder with a *cylindrical* PML. *Left:* Initial finite element mesh. *Right: hp*-refined mesh corresponding to 1% error and consisting of 8325 degrees-of-freedom. The color bar indicates the order of element edges and interiors.

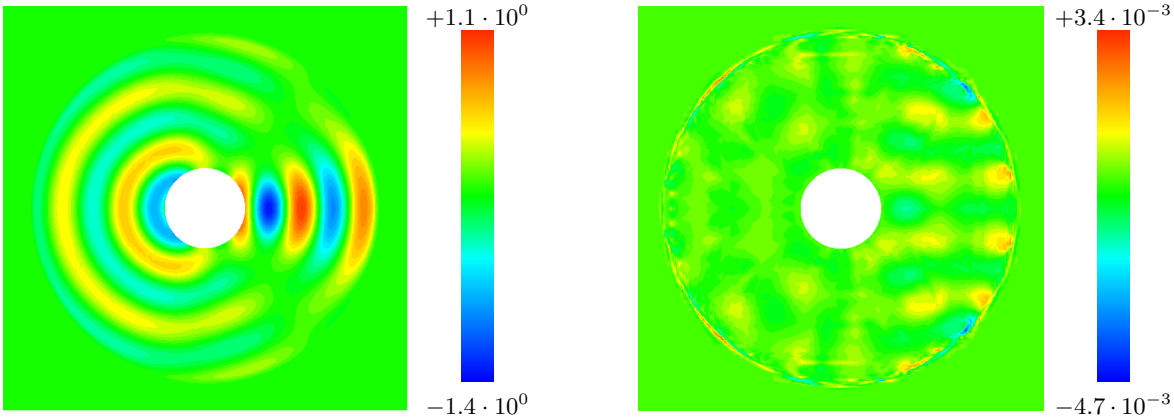

Figure 2: Acoustic scattering of a plane wave on a unit cylinder with a *cylindrical* PML. *Left:* Real component of the numerical solution. *Right:* Real component of the error function. Both the numerical solution and the error function were computed on the *hp* mesh given in Fig. 1 *(right)*.

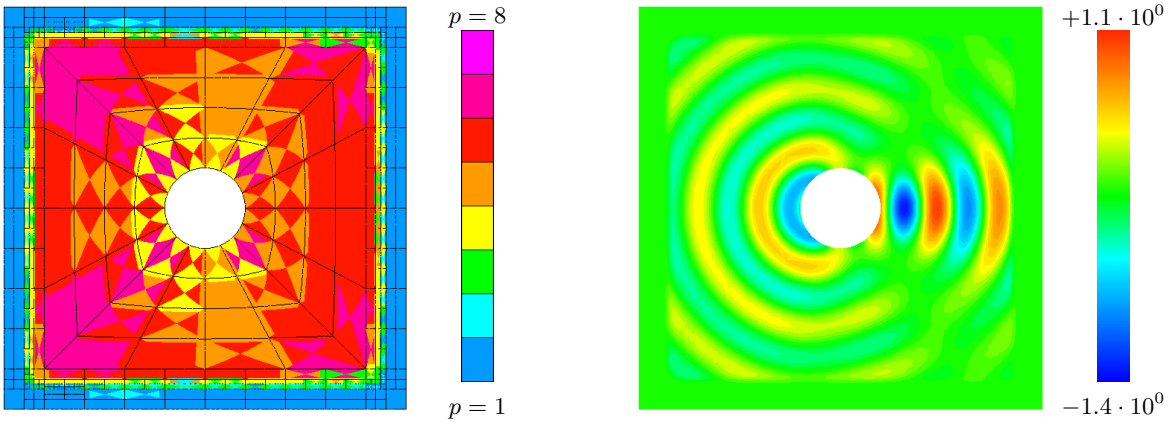

Figure 3: Acoustic scattering of a plane wave on a unit cylinder with a *Cartesian* PML. *Left: hp*-refined mesh corresponding to an error estimate of 1% and consisting of 4779 degrees-of-freedom. *Right:* Real component of the numerical solution computed on the *hp* mesh given in Fig. 3 *(left)*.

3D spherical PML

In this section, we consider a three-dimensional PML in spherical coordinates for the time-harmonic linear acoustics equations according to Eq. (2.18) with complex-coordinate stretching in the r coordinate only. To assess the effectiveness of the PML combined with *hp*-adaptivity, we compare its performance to the one of Infinite Elements; see e.g. Refs. [4, 12].

Below, we present numerical results for the scattering of a plane wave on a sphere with dimensionless radius $r = \lambda = 1$, where λ denotes the dimensionless wavelength. We set the dimensionless wavenumber $k = 2\pi$ and the direction of the incident wave $\boldsymbol{v} = (0, 0, -1)$. The computational domain is truncated by a spherical PML for $2 \leq r < 3$. In particular, we have employed coordinate stretching according to

$$z(r) = \begin{cases} r & 0 \leq r < 2 \\ r - iC(r-2)^6 & r \geq 2 \end{cases} \tag{2.24}$$

in order to have $z \in C^5$ globally, and the constant $C = -\log \epsilon$, where ϵ is the machine precision. Such a setting of C ensures that the analytic solution at the PML boundary is of the order of the machine precision and thus allows us to truncate the PML by a homogeneous Dirichlet boundary condition $p = 0$ at $r = 3$. The rigid scatterer is represented by the Neumann boundary condition $\partial p/\partial n = -\partial p^{\text{inc}}/\partial n$ on Γ_N, i.e. at $r = 1$, where $p^{\text{inc}} = e^{-ik\boldsymbol{v}\cdot\boldsymbol{x}}$ is the incident plane wave.

Figs. 5 *(left)* and *(right)* show cutaway views of two initial meshes used for comparison. Mesh (a) simply captures the geometry of the problem with the PML in the outer layer of elements. Mesh (b) includes one *h*-refinement in the radial direction. In Fig. 6 *(right)*, we plot the percent relative error in the H^1-seminorm (in a logarithmic scale) versus the total number of degrees-of-freedom N (in the algebraic scale $N^{1/3}$) for uniform $p = 2, \ldots, 9$ and both meshes (a) and (b). The error is evaluated only over the domain of interest $1 < r < 2$ with the exact solution (see e.g. [20, sec. 2.1.2]) used as a reference. We see that the radial *h*-refinement is essential, and that the curve for mesh (b) "looks like" exponential convergence with respect to p in this range. We also show convergence for the *p*-method when the PML in mesh (a) is replaced by infinite elements on the sphere $r = 2$. The exact solution is then analytic, and we observe exponential convergence in p, but *with a faster rate* than in the case with the PML. Finally, we apply our algorithm for fully-automatic *hp*-adaptivity (see [22]) with PML and using mesh (a) as the initial coarse grid. We plot the error for the first nine coarse grids and corresponding fine grids generated by the algorithm. The final coarse grid, shown in Fig. 6 *(left)*, achieves 0.6% relative error with 10K degrees-of-freedom, and the corresponding fine grid has 0.008%

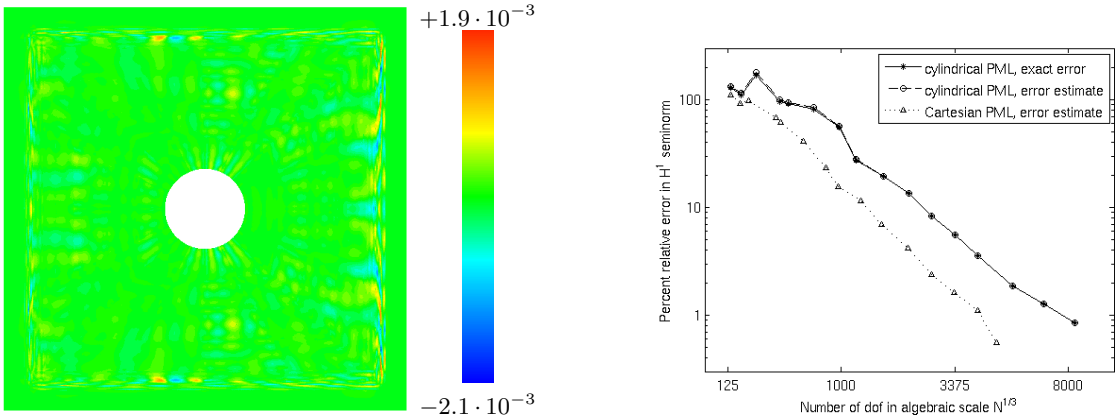

Figure 4: Acoustic scattering of a plane wave on a unit cylinder. *Left:* Real part of the error estimate for the case with *Cartesian* PML. *Right:* Percent relative error versus number of degrees-of-freedom for the cylindrical PML (exact error and error estimate) and for the Cartesian PML (error estimate).

relative error with 137K degrees-of-freedom. We note that the algorithm has automatically selected radial h-refinements within the PML, and that the convergence for the coarse grid appears to recover the rate delivered by infinite elements. In Figs. 7 *(left)* and *(right)*, we show the real component of the solution and of the error function, respectively.

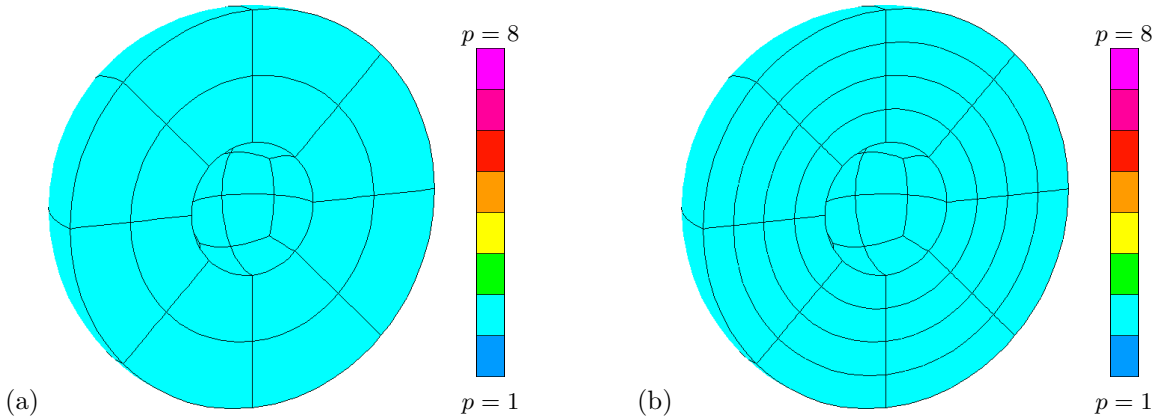

Figure 5: Acoustic scattering of a plane wave on a sphere. Two different initial grids for assessing the performance of a spherical PML and infinite elements.

3. Linear elasticity

In Section 3.1, we derive the PML formulation of the equations governing linear elasticity. In Section 3.2, we present numerical results that demonstrate the validity of the PML formulation for a two-layered elastic medium and the improvement in PML performance obtained by hp-adaptivity.

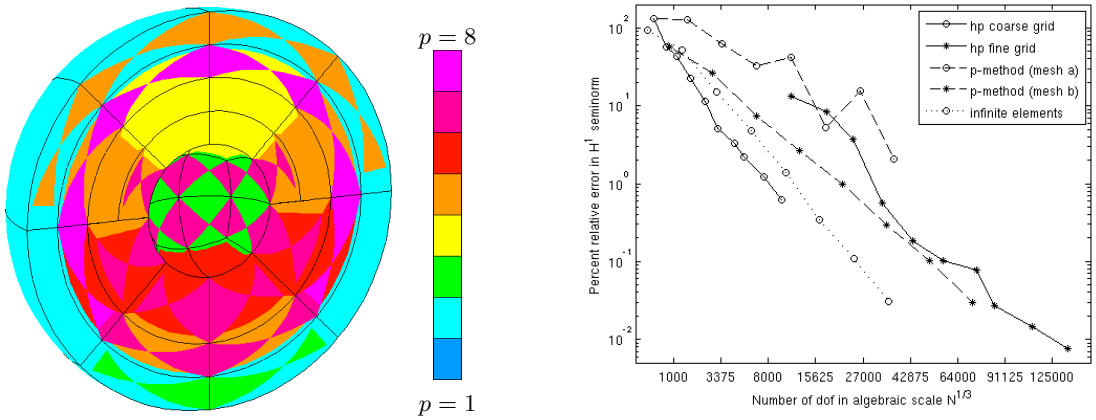

Figure 6: Acoustic scattering of a plane wave on a sphere. *Left:* *hp*-refined coarse mesh for the spherical PML after 9 iterations corresponding to 0.6% relative error and consisting of 10K degrees-of-freedom. *Right:* Comparison of *hp*-coarse and fine grids with the *p*-method for spherical PML and with the *p*-method for infinite elements.

3.1 PML formulation of the linear elasticity equations

In this section, we present the PML formulation for linear elasticity and discuss its implications. To this end, let us recall the equations of linear elasticity in $\mathbb{R}^n$ which, in time-harmonic form, are given by

$$\begin{cases} -\rho\omega^2 u_i - \sigma_{ij,j} = 0 & i = 1, \dots, n \\ \sigma_{ij} = E_{ijkl}\dfrac{1}{2}(u_{k,l} + u_{l,k}) & i, j = 1, \dots, n\,, \end{cases} \tag{3.25}$$

where u_i denotes the i-th component of the displacement vector, σ_{ij} is the stress tensor, ρ is the density and E_{ijkl} is the elasticity tensor satisfying the usual symmetry properties

$$E_{ijkl} = E_{jikl}, \quad E_{ijkl} = E_{ijlk}, \quad E_{ijkl} = E_{klij}\,. \tag{3.26}$$

The second symmetry property implies

$$E_{ijkl}\,\frac{1}{2}(u_{k,l} + u_{l,k}) = E_{ijkl}u_{k,l}\,. \tag{3.27}$$

For an isotropic homogeneous material, the elasticity tensor depends on two constants only, viz.

$$E_{ijkl} = \mu(\delta_{ik}\delta_{jl} + \delta_{il}\delta_{jk}) + \lambda\delta_{ij}\delta_{kl}\,, \tag{3.28}$$

where μ and λ are the Lamé constants and δ_{ij} is the Kronecker delta. In Eqs. (3.25)-(3.28) and throughout this section, we make use of the Einstein summation convention.

The system of equations (3.25) can be complemented by various boundary conditions of which we shall restrict ourselves to the simplest ones:

$$u_i = 0, \quad i = 1, \dots, n \quad \text{on}\,\Gamma_D\,, \tag{3.29a}$$

$$\sigma_{ij}n_j = g_i, \quad i = 1, \dots, n \quad \text{on}\,\Gamma_N\,, \tag{3.29b}$$

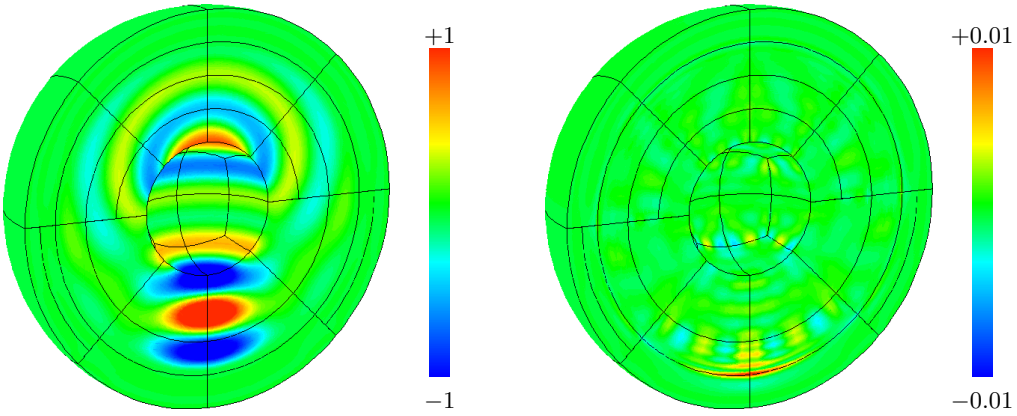

Figure 7: Acoustic scattering of a plane wave on a sphere. Real component of the numerical solution *(left)* and real component of the error function *(right)* computed on the *hp* mesh given in Fig. 6 *(left)* and using the spherical PML.

where n_j are the components of the outward normal unit vector, and g_i are prescribed tractions. Eq. (3.29a) prescribes zero displacements and corresponds to homogeneous Dirichlet boundary conditions, whereas Eq. (3.29b) prescribes given tractions and corresponds to Neumann boundary conditions.

To derive the standard variational formulation in terms of the displacement vector, we multiply the momentum equations $(3.25)_1$ with a test function $\boldsymbol{v} := v_i \in \boldsymbol{\mathcal{V}}$, integrate over the domain Ω and, upon integration-by-parts, we obtain

$$\int_\Omega \sigma_{ij} v_{i,j} \, d\Omega - \int_{\Gamma_N} \sigma_{ij} n_j v_i \, dS - \omega^2 \int_\Omega \rho u_i v_i \, d\Omega = 0 \,, \tag{3.30}$$

where we have tacitly restricted ourselves to test functions that satisfy homogeneous boundary conditions on the Dirichlet portion of the boundary, Γ_D. Substitution of the constitutive law $(3.25)_2$ and Neumann boundary condition (3.29b) into Eq. (3.30) then yields the final variational formulation

$$\left\{ \begin{array}{l} \boldsymbol{u} \in \boldsymbol{\mathcal{V}} \\ \displaystyle\int_\Omega E_{ijkl} u_{k,l} v_{i,j} \, d\Omega - \omega^2 \int_\Omega \rho u_i v_i \, d\Omega = \int_{\Gamma_N} g_i v_i \, dS, \\ \qquad\qquad\qquad\qquad\qquad\qquad \forall \boldsymbol{v} \in \boldsymbol{\mathcal{V}} \,, \end{array} \right. \tag{3.31}$$

where $\boldsymbol{\mathcal{V}}$ is the space of test functions

$$\boldsymbol{\mathcal{V}} := \{ \boldsymbol{v} \in \boldsymbol{\mathcal{X}} \, : \, \boldsymbol{v} = \boldsymbol{0} \text{ on } \Gamma_D \} \,, \tag{3.32}$$

which constitutes a subspace of the energy space $\boldsymbol{\mathcal{X}} := \boldsymbol{H}^1(\Omega)$.

Complex-coordinate stretching of the linear elasticity equations and derivation of the PML formulation is straightforward, and we shall thus discuss only the Cartesian form here. Under analytic continuation according to Eq. (2.6) with $x_j \to z_j(x_j)$, the elasticity equations (3.25) transform into

$$\left\{ \begin{array}{ll} \displaystyle -\rho z' \omega^2 u_i - \frac{z'}{z'_j} \sigma_{ij,j} = 0 & i = 1, \ldots, n \\ \displaystyle \sigma_{ij} = E_{ijkl} \frac{1}{z'_l} u_{k,l} & i,j = 1, \ldots, n \,, \end{array} \right. \tag{3.33}$$

where Eq. $(3.33)_1$ has been multiplied by $z' := \Pi_{j=1}^{n} z'_j$, which facilitates the subsequent integration-by-parts, since the prefactor z'/z'_j is independent of x_j.

The variational formulation of (3.33) can then be derived along the same lines as for the standard case considered in the beginning of this section, which yields

$$\begin{cases} \boldsymbol{u} \in \tilde{\boldsymbol{\mathcal{V}}}, \\ \displaystyle\int_\Omega \tilde{E}_{ijkl} u_{k,l} v_{i,j} \, d\Omega - \omega^2 \int_\Omega \tilde{\rho} u_i v_i \, d\Omega = \int_{\Gamma_N} g_i v_i \, dS, \\ \qquad\qquad\qquad\qquad\qquad\qquad \forall \boldsymbol{v} \in \tilde{\boldsymbol{\mathcal{V}}}\,, \end{cases} \tag{3.34}$$

where the "modified" elasticity tensor and density are given by

$$\tilde{E}_{ijkl} := E_{ijkl} \frac{z'}{z'_j z'_l} \qquad \text{(no summation)} \tag{3.35a}$$

$$\tilde{\rho} := \rho z' \,. \tag{3.35b}$$

In (3.34), the test space $\tilde{\boldsymbol{\mathcal{V}}}$ is a subspace of the energy space $\tilde{\boldsymbol{\mathcal{X}}}$ for the stretched variational form (3.34) which can be defined as

$$\tilde{\boldsymbol{\mathcal{V}}} := \{\boldsymbol{v} \in \tilde{\boldsymbol{\mathcal{X}}} \,:\, \boldsymbol{v} = \boldsymbol{0} \text{ on } \Gamma_D\} \tag{3.36}$$

with

$$\tilde{\boldsymbol{\mathcal{X}}} := \left\{ \boldsymbol{v} \,:\, \int_\Omega |\tilde{E}_{ijkl}| v_{k,l} \bar{v}_{i,j} \, d\Omega + \int_\Omega |\tilde{\rho}| v_i \bar{v}_i \, d\Omega < \infty \right\} \tag{3.37}$$

with the overbar denoting the complex conjugate. Hence, the energy space (3.37) corresponding to the variational form (3.34) is a weighted $\boldsymbol{H}^1$ space with weights that incorporate the derivatives of the stretching functions. Note that under complex-coordinate stretching the minor symmetries of the elasticity tensor (cf. (3.26)) are lost, which renders the elasticity tensor in the PML non-physical. However, since the major symmetry is retained, the bilinear form (3.34) is complex-symmetric.

Finally, let us point out that the formulation (3.34) is valid also for layered media with interfaces that are aligned with the Cartesian axes. This is a consequence of the fact that the solution remains analytic in terms of the coordinate parallel to the interface. We present numerical results demonstrating the validity of (3.34) for layered media in Section 3.2.

3.2 Numerical results for an elastic layered medium

In this section, we demonstrate the validity of the elasticity PML formulation (3.34) for layered media with interfaces that are aligned with the Cartesian axes. To this end, we consider a vibrating cylinder in a two-layered medium. Elastodynamic wave propagation in the presence of material layers is especially relevant for borehole geophysics applications; see e.g. Ref. [23].

We solve the linear elasticity equations on a rectangular domain $(-4, 4)^2$ with a circular hole of unit radius r in its center. The domain is surrounded by a Cartesian PML of unit thickness in which we apply complex-coordinate stretching according to

$$z_k(x_k) = \begin{cases} x_k & 0 \le |x_k| < 4 \\ \left(1 + \left(\frac{|x_k|-4}{0.5}\right)^5 - i\left(\frac{|x_k|-4}{0.5}\right)^5\right) x_k & |x_k| \ge 4 \end{cases} \qquad k = 1, 2\,. \tag{3.38}$$

Note that, in contrast to the complex-coordinate stretching that we used earlier in this work (see for instance Eq. (2.23)), the present form of stretching accounts also for the term $a_j(x_j)$ in accordance with Eq. (2.6) to accelerate the decay of evanescent waves in the PML; cf. also the discussion regarding the complex stretching in Section 2.2. Such evanescent waves are generated at the interface between the two material layers. This term in the stretching formula warrants that evanescent waves are

made to vanish in the PML before reaching the domain boundary. We remark that void of this term, spurious reflections of evanescent waves off the domain boundary would compromise convergence and accuracy.

Traction boundary conditions corresponding to a unit pressure are applied along the circumference of the hole, and homogeneous Dirichlet boundary conditions are applied on the outer domain boundary adjacent to the PML. The material data are given in terms of the Poisson ratio ν, the dimensionless density ρ and the dimensionless Young's modulus E

$$\nu = 0.3\,, \quad \rho = 1\,, \quad E = \begin{cases} 4 & x_2 \geq 0 \\ 1 & x_2 < 0 \end{cases} \,. \tag{3.39}$$

Moreover, we set $\omega = \pi$.

Starting from the same initial mesh as displayed in Fig. 1 *(left)*, an *hp*-refined mesh corresponding to an error estimate of 1% in the H^1-seminorm and consisting of 6508 degrees-of-freedom is obtained after 16 iterations; see Fig. 8 *(left)*. Observe the refinements that are selected by the adaptive algorithm, in particular in the PML layer to resolve the enforced rapid decay of the solution. In Fig. 8 *(right)*, we compare the convergence of *hp*-adaptive refinements and the simpler *h*-adaptive refinements with approximation degree $p = 2$ by plotting the percent relative error estimate in the H^1-seminorm (in a logarithmic scale) versus the total number of degrees-of-freedom N (in the algebraic scale $N^{1/3}$). The error estimate is obtained using the fine-grid solution as a reference solution and is evaluated over the entire computational domain including the PML. We remark that the *h*-adaptive refinement strategy allows for anisotropic refinements that are crucial for resolving the PML-induced gradients of the solution. Fig. 8 *(right)* indicates that both *hp*- and *h*-adaptive refinements deliver exponential convergence. Indeed, in the preasymptotic range, *h*-refinements can deliver exponential convergence before algebraic convergence sets in; cf. Ref. [11, ch. 14.3 and 14.4]. Note, however, that the convergence rates and error levels of *hp*- and *h*-refinements are significantly different. Hence, for a user-specified error tolerance, an *hp*-adaptive discretization is computationally much cheaper than an *h*-adaptive discretization. Moreover, it is obvious that for the resolution of PML-induced solution gradients an *h-uniform* discretization would be prohibitive in terms of computational cost. Our numerical results thus demonstrate that by means of *hp*-adaptivity reflections from the PML can be minimized to an arbitrary tolerance while retaining optimal accuracy for the least computational expense. In Figs. 9 *(left)* and *(right)*, we show the real component of the solution of the horizontal and vertical displacement, respectively, obtained on the *hp*-mesh given in Fig. 8 *(left)*. From Fig. 9 it is apparent that, in comparison with the greater Young's modulus for $x_2 \geq 0$, the smaller Young's modulus for $x_2 < 0$ results in a shorter wavelength of the solution and, thus, necessitates a finer *hp* discretization (see Fig. 8 *(left)*).

4. Maxwell's equations

In Section 4.1, we derive the PML formulation of Maxwell's equations in two-dimensional Cartesian coordinates. In Section 4.2, we present numerical results that demonstrate the improvement in performance of the PML for Maxwell's equations that can be obtained by using an *hp*-adaptive discretization.

4.1 PML formulation of Maxwell's equations in 2D Cartesian coordinates

To derive the PML formulation of Maxwell's equations, let us recall the time-harmonic form of Ampère's law and Faraday's law in three dimensions

$$(i\omega\epsilon + \sigma)\boldsymbol{E} - \boldsymbol{\nabla} \times \boldsymbol{H} = -\boldsymbol{J}^{\mathrm{imp}} \tag{4.40a}$$

$$i\omega\mu\boldsymbol{H} + \boldsymbol{\nabla} \times \boldsymbol{E} = \boldsymbol{0}\,, \tag{4.40b}$$

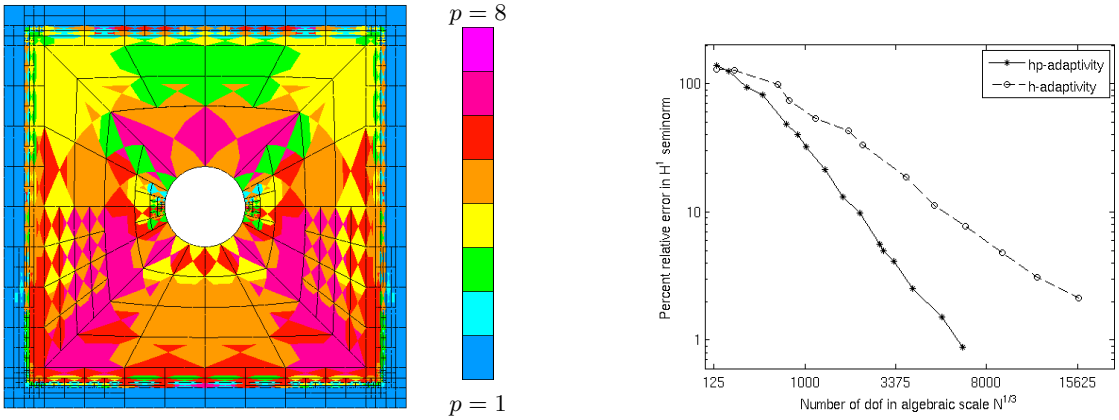

Figure 8: Wave propagation in an elastic two-layered medium. *Left: hp*-mesh corresponding to an error estimate of 1% and consisting of 6508 degrees-of-freedom. *Right:* Percent relative error estimate versus number of degrees-of-freedom for *hp*-adaptive and *h*-adaptive refinement.

respectively. In (4.40), $\boldsymbol{E}$ and $\boldsymbol{H}$ denote the electric and magnetic field vector, respectively, ω is the angular frequency, μ, ϵ and σ are the permeability, permittivity and conductivity, respectively, $\boldsymbol{J}^{\text{imp}}$ is a given impressed volume current, and i denotes the imaginary unit.

Eqs. (4.40) invoke the curl operator which, in Cartesian coordinates, is expressed as

$$\boldsymbol{\nabla} \times \boldsymbol{E} = \left(\frac{\partial E_3}{\partial x_2} - \frac{\partial E_2}{\partial x_3} \,, \frac{\partial E_1}{\partial x_3} - \frac{\partial E_3}{\partial x_1} \,, \frac{\partial E_2}{\partial x_1} - \frac{\partial E_1}{\partial x_2} \right) . \tag{4.41}$$

In this section, we shall confine ourselves to Maxwell's equations in two dimensions. However, for future reference, we include the PML derivation for the three-dimensional Maxwell's equations in Appendix C. For a vector-valued two-dimensional electric field $\boldsymbol{E} = (E_1, E_2, 0)$ with components that depend only on x_1, x_2, only the third component of the three-dimensional curl operator is different from zero

$$\boldsymbol{\nabla} \times \boldsymbol{E} = \left(0 \,, 0 \,, \frac{\partial E_2}{\partial x_1} - \frac{\partial E_1}{\partial x_2} \right) . \tag{4.42}$$

Accordingly, we shall define a two-dimensional scalar-valued curl operator as

$$\text{curl}\boldsymbol{E} := \frac{\partial E_2}{\partial x_1} - \frac{\partial E_1}{\partial x_2} \,. \tag{4.43}$$

Similarly, for a scalar-valued one-dimensional magnetic field $\boldsymbol{H} = (0, 0, H_3)$ the curl operator reduces to

$$\boldsymbol{\nabla} \times \boldsymbol{H} = \left(\frac{\partial H_3}{\partial x_2} \,, -\frac{\partial H_3}{\partial x_1} \,, 0 \right) . \tag{4.44}$$

Invoking Eqs. (4.41)-(4.44), the two-dimensional Maxwell's equations in time-harmonic form follow from (4.40)

$$\begin{cases} i\omega\epsilon E_1 + \sigma E_1 - \dfrac{\partial H_3}{\partial x_2} & = -J_1^{\text{imp}} \\ i\omega\epsilon E_2 + \sigma E_2 + \dfrac{\partial H_3}{\partial x_1} & = -J_2^{\text{imp}} \\ i\omega\mu H_3 + \dfrac{\partial E_2}{\partial x_1} - \dfrac{\partial E_1}{\partial x_2} & = 0 \,. \end{cases} \tag{4.45}$$

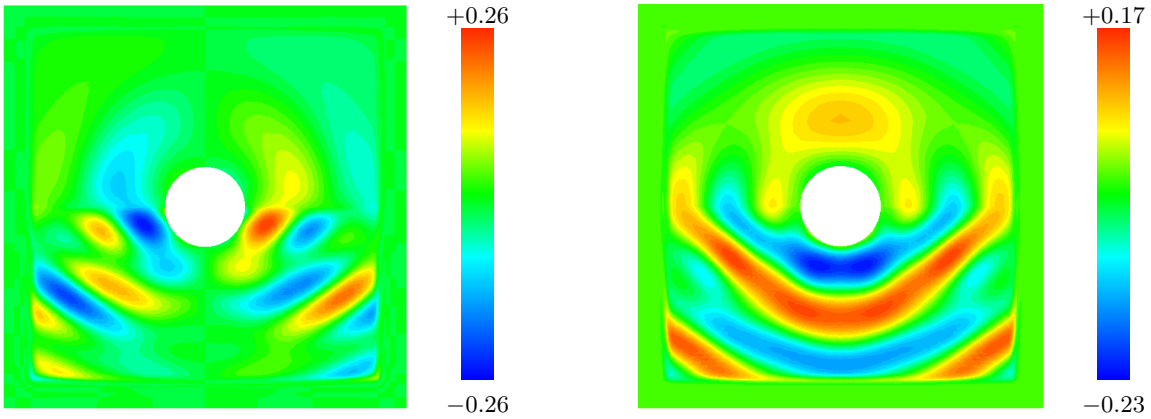

Figure 9: Wave propagation in an elastic two-layered medium. Real component of the horizontal displacement *(left)* and of the vertical displacement *(right)*.

If the solution is analytic in x_1 and x_2, the Cartesian coordinates x_1 and x_2 can be replaced by the complex coordinates z_1 and z_2, respectively, and the derivatives can be interpreted in the complex sense. Under complex-coordinate stretching according to (2.6) with $x_j \to z_j(x_j)$, Eqs. (4.45) transform into

$$\begin{cases} (i\omega\epsilon + \sigma)E_1 - \dfrac{1}{z_1' z_2'}\dfrac{\partial(z_1' H_3)}{\partial x_2} &= -J_1^{\text{imp}} \\ (i\omega\epsilon + \sigma)E_2 + \dfrac{1}{z_1' z_2'}\dfrac{\partial(z_2' H_3)}{\partial x_1} &= -J_2^{\text{imp}} \\ i\omega\mu H_3 + \dfrac{1}{z_1' z_2'}\dfrac{\partial(z_2' E_2)}{\partial x_1} - \dfrac{1}{z_1' z_2'}\dfrac{\partial(z_1' E_1)}{\partial x_2} &= 0\,, \end{cases} \tag{4.46}$$

where we have made use of the fact that the j-th complex coordinate depends only on the j-th real coordinate, $z_j = z_j(x_j)$. Upon multiplication of Eq. $(4.46)_1$ by $i\omega z_1' z_2' F_1$ and Eq. $(4.46)_2$ by $i\omega z_1' z_2' F_2$ with $\boldsymbol{F} := (F_1, F_2)$ a test function, integration over domain Ω and integration-by-parts, we obtain

$$\begin{aligned} &\int_\Omega (-\omega^2\epsilon + i\omega\sigma)\left(\frac{z_2'}{z_1'}(z_1' E_1)(z_1' F_1) + \frac{z_1'}{z_2'}(z_2' E_2)(z_2' F_2)\right) d\Omega + \int_\Omega i\omega H_3 \left(\frac{\partial(z_1' F_1)}{\partial x_2} - \frac{\partial(z_2' F_2)}{\partial x_1}\right) d\Omega \\ &\quad + \int_{\partial\Omega} i\omega H_3 (z_1' F_1(-n_2) + z_2' F_2 n_1)\, dS = -i\omega \int_\Omega (z_2' J_1^{\text{imp}}(z_1' F_1) + z_1' J_2^{\text{imp}}(z_2' F_2))\, d\Omega\,, \end{aligned} \tag{4.47}$$

where $\boldsymbol{n} = (n_1, n_2)$ denotes the outward normal unit vector. Integrability considerations imply that the "generalized tangential component" in Eq. (4.47),

$$F_t := z_1' F_1(-n_2) + z_2' F_2 n_1\,, \tag{4.48}$$

must be continuous across inter-element boundaries.

Substituting Eq. $(4.46)_3$ into (4.47) and assuming firstly, a nonhomogeneous Dirichlet boundary condition on the physical boundary

$$\boldsymbol{n} \times \boldsymbol{E} = -\boldsymbol{n} \times \boldsymbol{E}^{\text{inc}} \tag{4.49}$$

with $\boldsymbol{E}^{\text{inc}}$ a prescribed incident wave, secondly, a homogeneous Dirichlet boundary condition on the PML boundary

$$z_1' E_1(-n_2) + z_2' E_2 n_1 = 0\,, \tag{4.50}$$

and thirdly, a homogeneous boundary condition for the test function on the entire boundary

$$F_t = 0\,, \tag{4.51}$$

we obtain the final variational statement

$$\begin{aligned}\int_\Omega \frac{1}{\mu z_1' z_2'} \left(\frac{\partial(z_2' E_2)}{\partial x_1} - \frac{\partial(z_1' E_1)}{\partial x_2}\right)\left(\frac{\partial(z_2' F_2)}{\partial x_1} - \frac{\partial(z_1' F_1)}{\partial x_2}\right) d\Omega \\ - \int_\Omega (\omega^2\epsilon - i\omega\sigma)\left(\frac{z_2'}{z_1'}(z_1' E_1)(z_1' F_1) + \frac{z_1'}{z_2'}(z_2' E_2)(z_2' F_2)\right) d\Omega \\ = -i\omega \int_\Omega \left(z_2' J_1^{\mathrm{imp}}(z_1' F_1) + z_1' J_2^{\mathrm{imp}}(z_2' F_2)\right) d\Omega \quad \forall \boldsymbol{F}\,. \end{aligned} \tag{4.52}$$

We now redefine the variables

$$E_j \leftarrow z_j' E_j, \quad j = 1, 2\,, \tag{4.53a}$$

$$F_j \leftarrow z_j' F_j, \quad j = 1, 2\,. \tag{4.53b}$$

Note that the factor z_j' grows algebraically in the PML, whereas the solution E_j decays exponentially. Therefore, the redefined variables will eventually also decay exponentially in the PML, but an initial algebraic growth may be observed. In terms of the redefined variables, Eq. (4.52) assumes the standard form

$$\begin{cases} \boldsymbol{E} \in \hat{\boldsymbol{E}} + \tilde{\boldsymbol{\mathcal{F}}} \\ \displaystyle\int_\Omega \left(\frac{1}{\mu z_1' z_2'} \operatorname{curl}\boldsymbol{E} \operatorname{curl}\boldsymbol{F} - (\omega^2\epsilon - i\omega\sigma)\left(\frac{z_2'}{z_1'} E_1 F_1 + \frac{z_1'}{z_2'} E_2 F_2\right)\right) d\Omega \\ \qquad = -i\omega \displaystyle\int_\Omega \left(z_2' J_1^{\mathrm{imp}} F_1 + z_1' J_2^{\mathrm{imp}} F_2\right) d\Omega \\ \qquad\qquad \forall \boldsymbol{F} \in \tilde{\boldsymbol{\mathcal{F}}}\,. \end{cases} \tag{4.54}$$

Note that problem (4.54) is complex symmetric. In Eq. (4.54), $\hat{\boldsymbol{E}}$ denotes a lift of the Dirichlet data, and the test space $\tilde{\boldsymbol{\mathcal{F}}}$ is a subspace of the "energy space" $\tilde{\boldsymbol{\mathcal{X}}}$ for the stretched variational form (4.54) which can be defined as

$$\tilde{\boldsymbol{\mathcal{F}}} := \{\boldsymbol{F} \in \tilde{\boldsymbol{\mathcal{X}}} \;:\; F_t = 0 \text{ on } \partial\Omega\} \tag{4.55}$$

with

$$\tilde{\boldsymbol{\mathcal{X}}} := \left\{ \boldsymbol{F} \;:\; \left|\frac{z_2'}{z_1'}\right|^{\frac{1}{2}} F_1,\, \left|\frac{z_1'}{z_2'}\right|^{\frac{1}{2}} F_2,\, \frac{1}{|z_1' z_2'|^{\frac{1}{2}}} \operatorname{curl}\boldsymbol{F} \in L^2(\Omega) \right\}. \tag{4.56}$$

Note that the "energy space" $\tilde{\boldsymbol{\mathcal{X}}}$ is a weighted $\boldsymbol{H}(\mathrm{curl})$ space with weights associated with the derivatives of the stretching functions.

We emphasize that the redefinition of the variables according to (4.53) is not merely a convenience. Integrability assumptions in conformity with (4.56) imply continuity of the tangential component F_t of the redefined variable across interelement boundaries and, consequently, the redefinition (4.53) enables discretization with $\boldsymbol{H}(\mathrm{curl})$-conforming elements. Moreover, let us point out that the redefined variables satisfy the original Maxwell's equations and, consequently, the variational statement (4.54) assumes the usual form associated with Maxwell's equations. Therefore, this form of PML is typically also referred to as *Maxwellian* PML; see e.g. Ref. [30].

4.2 Numerical experiments

In this section, we demonstrate the validity of the PML formulation for Maxwell's equations, Eq. (4.54), and the benefit of *hp*-adaptivity for improving the PML performance. To this end, we consider the scattering of a plane wave on a cylinder.

We solve Maxwell's equations on a rectangular domain $(-4,4)^2$ with a circular hole of unit radius in its center. The domain is surrounded by a PML of unit thickness in which complex-coordinate stretching according to

$$z_k(x_k) = \begin{cases} x_k & 0 \le |x_k| < 4 \\ x_k - i\left(\frac{|x_k|-4}{0.5}\right)^5 x_k & |x_k| \ge 4 \end{cases} \qquad k = 1,2 \tag{4.57}$$

is invoked. Dirichlet boundary conditions corresponding to an incident plane wave $\boldsymbol{E}^{\text{inc}} = \boldsymbol{p}e^{-ik\boldsymbol{v}\cdot\boldsymbol{x}}$ are applied along the circumference of the cylinder, and homogeneous Dirichlet boundary conditions are applied on the outer domain boundary adjacent to the PML. The physical parameters are given in Table 1, where $\boldsymbol{v}$ and $\boldsymbol{p}$ denote the direction and the polarization of the incident wave, respectively, and r is the cylinder radius. With the parameters specified in Table 1, the speed of light is $c = 1/\sqrt{\mu\epsilon} = 1$ and the wavenumber is $k = \omega/c = 2\pi$.

Table 1: Physical parameters.

ω	r	$\boldsymbol{v}$	$\boldsymbol{p}$	μ	ϵ	σ
2π	1	$(-1,0)$	$(0,1)$	1	1	0

Starting from the same initial mesh as displayed in Fig. 1 *(left)*, an *hp*-refined mesh corresponding to an error estimate of 1% in the $\boldsymbol{H}$(curl)-seminorm and consisting of 14664 degrees-of-freedom is obtained after 16 iterations; see Fig. 10 *(left)*. Note the refinements that are selected by the adaptive algorithm, in particular in the PML layer. In Fig. 10 *(right)*, we show the real part of the second component of the solution obtained on the *hp*-mesh given in Fig. 10 *(left)*. The corresponding error estimate, i.e. the difference between the coarse and fine grid solution, is shown in Fig. 11 *(left)*. We remark that, in contrast to acoustics or elasticity problems, the solution to the PML-modified Maxwell's equations may exhibit an initial growth in the PML domain. To support this claim, we display in Fig. 11 *(right)* the real part of the second component of the solution for a wavenumber $k = 1$. The initial growth in the PML domain is caused by the fact that we have chosen to discretize the modified variable $(z_1' E_1, z_2' E_2)$ rather than (E_1, E_2) directly. In the PML, the stretching coefficients z_i initially grow algebraically, whereas the solution E_i decays exponentially. Therefore, the modified variable $(z_1' E_1, z_2' E_2)$ also grows initially before it exhibits the exponential decay.

5. Conclusion

In this work, we improved the performance of the Perfectly Matched Layer by using an automatic *hp*-adaptive discretization. The PML has the remarkable property of having a zero reflection coefficient for all angles of incidence and all frequencies on the continuum level. However, this property is compromised under discretization, i.e. at a discrete PML spurious reflections typically do occur. Only for vanishing mesh size, i.e. upon convergence to the continuum solution, the property of having a zero reflection coefficient can be recovered. By means of an automatic *hp*-adaptive discretization, we obtain a sequence of discrete solutions that converges exponentially to the continuum solution. This allows us to minimize reflections from the discrete PML to an arbitrary level of accuracy. The strength of our *hp*-adaptive discretization is that it can effectively resolve the strong PML-induced gradients of the solution by adapting the element size h and polynomial approximation order p for any given PML profile. Since the *hp*-adaptivity is automatic, no interaction with the user is required. This renders tedious parameter tuning of the PML obsolete.

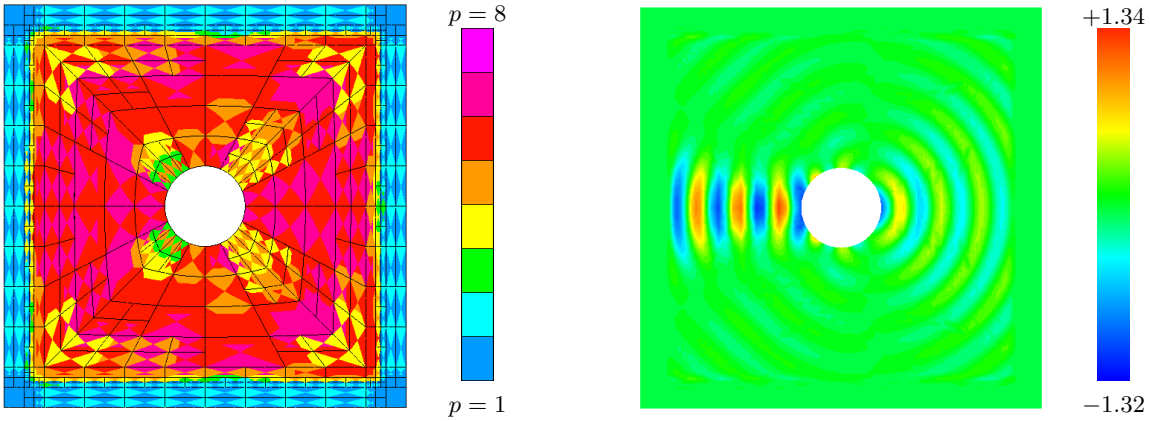

Figure 10: Electromagnetic scattering of a plane wave on a cylinder. *Left:* *hp*-refined mesh corresponding to an error estimate of 1% and consisting of 14664 degrees-of-freedom; $k = 2\pi$. *Right:* Real part of the second component of the numerical solution; $k = 2\pi$.

We demonstrated the improvement of the PML performance by *hp*-adaptivity and the versatility of this approach by numerical results for acoustic, elastodynamic and electromagnetic wave-propagation problems in the frequency domain and in different systems of coordinates. Our results show that *hp*-adaptivity minimizes reflections from the PML to an arbitrary level of accuracy while retaining optimal computational efficiency. Moreover, we showed that *hp*-adaptivity provides the freedom to select the geometry of the PML independently of the geometry of the initial mesh, i.e. the respective geometries need not coincide. Our results suggest that *hp*-adaptivity is ideally suited for improving the performance of the PML and, conversely, the PML is the ideal absorbing boundary condition for *hp*-adaptive finite-element methods.

Acknowledgements

The first author was supported by the Netherlands Organization for Scientific Research (NWO) and the ICES Postdoctoral Fellowship Program of the Institute for Computational Engineering and Sciences (ICES) at The University of Texas at Austin. The second and third author were supported by Air Force under Contract FA9550-04-1-0050. The fourth author was supported by Baker Atlas and The University of Texas at Austin's *Joint Industry Research Consortium on Formation Evaluation*. This support is gratefully acknowledged.

Moreover, the second author wishes to thank Prof. Joachim Schöberl, RWTH Aachen, Germany for an inspiring discussion about the Perfectly Matched Layer.

A. Derivation of the PML formulation for the Helmholtz equation in 2D polar coordinates

In the sequel, we derive the PML formulation for the Helmholtz equation in two dimensions and polar coordinates which leads to the variational statement (2.13) that is given in Section 2.3.

Recalling the formulas for the gradient of a scalar p and for the divergence of a vector field $\boldsymbol{u} = u_r \boldsymbol{e}_r + u_\theta \boldsymbol{e}_\theta$ in polar coordinates

$$\boldsymbol{\nabla} p = \frac{\partial p}{\partial r}\boldsymbol{e}_r + \frac{1}{r}\frac{\partial p}{\partial \theta}\boldsymbol{e}_\theta \,, \tag{A.58a}$$

$$\boldsymbol{\nabla} \cdot \boldsymbol{u} = \frac{1}{r}\frac{\partial}{\partial r}(r u_r) + \frac{1}{r}\frac{\partial u_\theta}{\partial \theta} \,, \tag{A.58b}$$

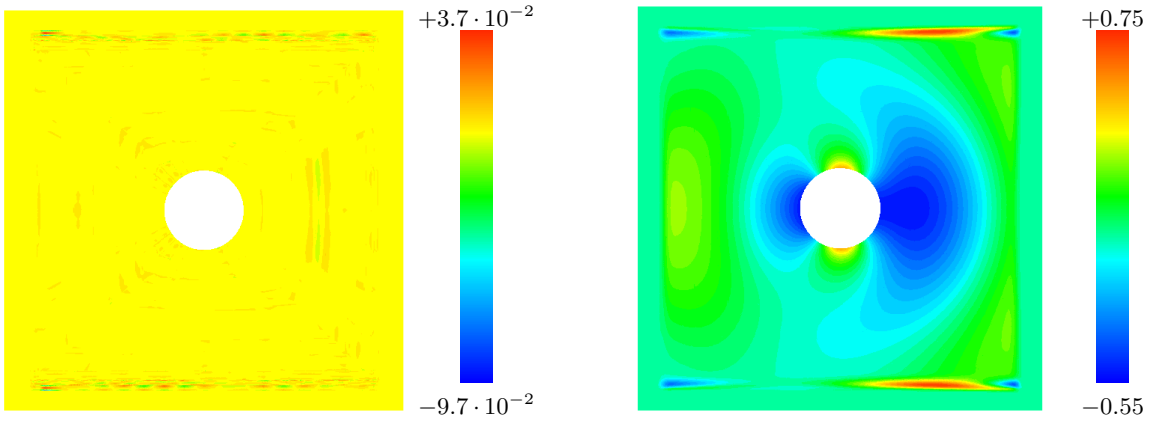

Figure 11: Electromagnetic scattering of a plane wave on a cylinder. *Left:* Real part of the second component of the error estimate; $k = 2\pi$. *Right:* Real part of the second component of the numerical solution; $k = 1$.

respectively, we convert the first-order system of linear acoustics equations (2.5) to polar coordinates

$$\begin{cases} i\omega p + \rho_0 c^2 \left(\dfrac{1}{r} \dfrac{\partial}{\partial r}(r u_r) + \dfrac{1}{r} \dfrac{\partial u_\theta}{\partial \theta} \right) & = 0 \\ i\omega \rho_0 u_r + \dfrac{\partial p}{\partial r} & = 0 \\ i\omega \rho_0 u_\theta + \dfrac{1}{r} \dfrac{\partial p}{\partial \theta} & = 0 \,. \end{cases} \tag{A.59}$$

Introducing in (A.59) complex-coordinate stretching according to (2.6) with $r \to z(r)$ yields

$$\begin{cases} i\omega p + \rho_0 c^2 \left(\dfrac{1}{z' z} \dfrac{\partial}{\partial r}(z u_r) + \dfrac{1}{z} \dfrac{\partial u_\theta}{\partial \theta} \right) & = 0 \\ i\omega \rho_0 u_r + \dfrac{1}{z'} \dfrac{\partial p}{\partial r} & = 0 \\ i\omega \rho_0 u_\theta + \dfrac{1}{z} \dfrac{\partial p}{\partial \theta} & = 0 \,. \end{cases} \tag{A.60}$$

Multiplying Eq. $(A.60)_1$ by $i\omega z' z / r$ and subsequently by a test function q, integrating the resulting expression over domain Ω and integrating by parts, we obtain

$$-\omega^2 \int_\Omega \frac{z' z}{r} pq \, r dr d\theta - i\omega \rho_0 c^2 \int_\Omega \left(\frac{z}{r} u_r \frac{\partial q}{\partial r} + \frac{z'}{r} u_\theta \frac{\partial q}{\partial \theta} \right) r dr d\theta = 0 \,, \tag{A.61}$$

where we tacitly assumed Dirichlet boundary conditions for the solution on the entire boundary, Γ, and, accordingly, homogeneous boundary conditions for the test function q. To eliminate the velocity components u_r and u_θ from Eq. (A.61), we substitute Eqs. $(A.60)_{2,3}$ into (A.61), and obtain the final variational formulation (2.13).

B. Derivation of the PML formulation for the Helmholtz equation in 3D spherical coordinates

In the sequel, we derive the PML formulation for the Helmholtz equation in three dimensions and spherical coordinates which leads to the variational statement (2.18) that is given in Section 2.4.

Recalling the formulas for the gradient of a scalar p and the divergence of a vector field $\boldsymbol{u} = u_r\boldsymbol{e}_r + u_\psi\boldsymbol{e}_\psi + u_\theta\boldsymbol{e}_\theta$ in spherical coordinates

$$\boldsymbol{\nabla} p = \frac{\partial p}{\partial r}\boldsymbol{e}_r + \frac{1}{r}\frac{\partial p}{\partial \psi}\boldsymbol{e}_\psi + \frac{1}{r\sin\psi}\frac{\partial p}{\partial \theta}\boldsymbol{e}_\theta\,, \tag{B.62a}$$

$$\boldsymbol{\nabla}\cdot\boldsymbol{u} = \frac{1}{r^2}\frac{\partial}{\partial r}(r^2 u_r) + \frac{1}{r\sin\psi}\frac{\partial}{\partial \psi}(u_\psi \sin\psi) + \frac{1}{r\sin\psi}\frac{\partial u_\theta}{\partial \theta}\,, \tag{B.62b}$$

we convert the first-order system of linear acoustics equations (2.5) to spherical coordinates

$$\left\{\begin{aligned} i\omega p + \rho_0 c^2\left(\frac{1}{r^2}\frac{\partial}{\partial r}(r^2 u_r) + \frac{1}{r\sin\psi}\frac{\partial}{\partial \psi}(u_\psi\sin\psi) + \frac{1}{r\sin\psi}\frac{\partial u_\theta}{\partial\theta}\right) &= 0\\ i\omega\rho_0 u_r + \frac{\partial p}{\partial r} &= 0\\ i\omega\rho_0 u_\psi + \frac{1}{r}\frac{\partial p}{\partial\psi} &= 0\\ i\omega\rho_0 u_\theta + \frac{1}{r\sin\psi}\frac{\partial p}{\partial\theta} &= 0\,. \end{aligned}\right. \tag{B.63}$$

In spherical coordinates, the reflectionless absorption of outward traveling waves can be achieved through analytic continuation on the radial variable r according to Eq. (2.6) with $r \to z(r)$. This transforms Eq. (B.63) into

$$\left\{\begin{aligned} i\omega p + \rho_0 c^2\left(\frac{1}{z'z^2}\frac{\partial}{\partial r}(z^2 u_r) + \frac{1}{z\sin\psi}\frac{\partial}{\partial \psi}(u_\psi\sin\psi) + \frac{1}{z\sin\psi}\frac{\partial u_\theta}{\partial\theta}\right) &= 0\\ i\omega\rho_0 u_r + \frac{1}{z'}\frac{\partial p}{\partial r} &= 0\\ i\omega\rho_0 u_\psi + \frac{1}{z}\frac{\partial p}{\partial\psi} &= 0\\ i\omega\rho_0 u_\theta + \frac{1}{z\sin\psi}\frac{\partial p}{\partial\theta} &= 0\,. \end{aligned}\right. \tag{B.64}$$

We multiply Eq. $(\text{B.64})_1$ by $i\omega z'z^2/r^2$ and then by a test function q, and we integrate the resulting expression over the domain Ω, which yields

$$\begin{aligned} &-\omega^2\int_\Omega z'\frac{z^2}{r^2}pq\, r^2\sin\psi dr d\psi d\theta\\ &+ i\omega\rho_0 c^2\int_\Omega\left(\frac{1}{r^2}\frac{\partial}{\partial r}(z^2u_r)q + \frac{z'z}{r^2\sin\psi}\frac{\partial}{\partial\psi}(u_\psi\sin\psi)q + \frac{z'z}{r^2\sin\psi}\frac{\partial u_\theta}{\partial\theta}q\right) r^2\sin\psi dr d\psi d\theta = 0\,. \end{aligned} \tag{B.65}$$

Upon integrating Eq. (B.65) by parts and eliminating u_r, u_ψ and u_θ by invoking Eqs. $(\text{B.64})_{2,3,4}$, respectively, we obtain the final variational formulation (2.18).

C. PML formulation of Maxwell's equations in 3D Cartesian coordinates

As an extension of Section 4.1, we derive in the sequel the PML formulation for Maxwell's equations in three dimensions and Cartesian coordinates. To this end, it is convenient to rewrite the time-harmonic form of Ampère's and Faraday's law, Eqs. (4.40a) and (4.40b), respectively, expressing the curl operator by means of the permutation symbol ε_{ijk} that is defined as

$$\varepsilon_{ijk} := \left\{\begin{aligned} 0\,, &\quad \text{if any two indices are repeated}\\ 1\,, &\quad \text{if } ijk \text{ is an even permutation of } 123\\ -1\,, &\quad \text{if } ijk \text{ is an odd permutation of } 123 \end{aligned}\right., \tag{C.66}$$

which then yields

$$\begin{aligned} (i\omega\epsilon+\sigma)E_i - \sum_{j,k}\varepsilon_{ijk}H_{k,j} &= -J_i^{\mathrm{imp}} && i=1,2,3 \\ i\omega\mu H_k + \sum_{m,n}\epsilon_{kmn}E_{n,m} &= 0 && k=1,2,3\,, \end{aligned} \tag{C.67}$$

respectively. Mind that in this section, we write sums explicitly using the summation symbol, rather than making use of the Einstein summation convention. Under complex-coordinate stretching according to Eq. (2.6) with $x_i \to z_i(x_i)$, system (C.67) transforms into

$$(i\omega\epsilon+\sigma)E_i - \sum_{j,k}\varepsilon_{ijk}\frac{1}{z_j'}H_{k,j} = -J_i^{\mathrm{imp}} \tag{C.68a}$$

$$i\omega\mu H_k + \sum_{m,n}\epsilon_{kmn}\frac{1}{z_m'}E_{n,m} = 0\,. \tag{C.68b}$$

Upon multiplication of Eq. (C.68a) by $z' := z_1' z_2' z_3'$, we obtain

$$(i\omega\epsilon+\sigma)\frac{z'}{z_i'}(z_i'E_i) - \sum_{j,k}\varepsilon_{ijk}\frac{z'}{z_j'}H_{k,j} = -z'J_i^{\mathrm{imp}}\,. \tag{C.69}$$

We then multiply Eq. (C.69) by a test function F_i, integrate over a domain Ω and integrate by parts, which yields

$$\begin{aligned} \int_\Omega \left((i\omega\epsilon+\sigma)\frac{z'}{(z_i')^2}(z_i'E_i)(z_i'F_i) + \sum_{j,k}\varepsilon_{ijk}\frac{z'}{z_i'z_j'}H_k(z_i'F_i)_{,j}\right) d\Omega \\ = -\int_\Omega \frac{z'}{z_i'}J_i^{\mathrm{imp}}(z_i'F_i)\,d\Omega + \int_{\partial\Omega}\sum_{j,k}\varepsilon_{ijk}\frac{z'}{z_i'z_j'}H_k(z_i'F_i)n_j\,dS\,. \end{aligned} \tag{C.70}$$

Next, we multiply Eq. (C.70) by $i\omega$ and eliminate H_k from the volume integral by invoking (C.68b)

$$\begin{aligned} \int_\Omega \left((-\omega^2\epsilon+i\omega\sigma)\frac{z'}{(z_i')^2}(z_i'E_i)(z_i'F_i) - \frac{1}{\mu}\sum_{j,k}\varepsilon_{ijk}\frac{z'}{z_i'z_j'}\sum_{m,n}\epsilon_{kmn}\frac{1}{z_n'z_m'}(z_n'E_n)_{,m}(z_i'F_i)_{,j}\right) d\Omega \\ = -i\omega\int_\Omega \frac{z'}{z_i'}J_i^{\mathrm{imp}}(z_i'F_i)\,d\Omega + i\omega\int_{\partial\Omega}\sum_{j,k}\varepsilon_{ijk}\frac{z'}{z_i'z_j'}H_k(z_i'F_i)n_j\,dS\,. \end{aligned} \tag{C.71}$$

Summation over index i and some straightforward algebraic manipulations then yield

$$\begin{aligned} \int_\Omega \left((-\omega^2\epsilon+i\omega\sigma)\sum_i \frac{z'}{(z_i')^2}(z_i'E_i)(z_i'F_i) - \frac{z'}{\mu}\sum_k\left(\sum_{m,n}\epsilon_{kmn}\frac{1}{z_n'z_m'}(z_n'E_n)_{,m}\right)\left(\sum_{i,j}\epsilon_{kij}\frac{1}{z_i'z_j'}(z_i'F_i)_{,j}\right)\right) d\Omega \\ = -i\omega\int_\Omega\sum_i \frac{z'}{z_i'}J_i^{\mathrm{imp}}(z_i'F_i)\,d\Omega + i\omega\int_{\partial\Omega}\sum_{i,j,k}\varepsilon_{ijk}\frac{z'}{z_i'z_j'}H_k(z_i'F_i)n_j\,dS\,. \end{aligned} \tag{C.72}$$

Upon redefining the variables

$$E_i \leftarrow z_i'E_i, \quad i=1,2,3\,, \tag{C.73a}$$

$$H_i \leftarrow z_i' H_i, \quad i = 1,2,3\,, \tag{C.73b}$$

$$F_i \leftarrow z_i' F_i, \quad i = 1,2,3\,, \tag{C.73c}$$

and incorporating into Eq. (C.72) a Neumann boundary condition with $J_{S,i}^{\text{imp}}$ an impressed surface current, we obtain the final variational formulation

$$\begin{cases} \boldsymbol{E} \in \hat{\boldsymbol{E}} + \tilde{\boldsymbol{\mathcal{F}}} \\ \displaystyle\int_\Omega \left((-\omega^2\epsilon + i\omega\sigma) \sum_i \frac{z'}{(z_i')^2} E_i F_i - \frac{z'}{\mu} \sum_k \left(\sum_{m,n} \epsilon_{kmn} \frac{1}{z_n' z_m'} E_{n,m} \right) \left(\sum_{i,j} \epsilon_{kij} \frac{1}{z_i' z_j'} F_{i,j} \right) \right) d\Omega \\ \qquad = -i\omega \displaystyle\int_\Omega \sum_i \frac{z'}{z_i'} J_i^{\text{imp}} F_i \, d\Omega + i\omega \int_{\Gamma_N} \sum_i J_{S,i}^{\text{imp}} F_i \, dS \\ \qquad\qquad \forall \boldsymbol{F} \in \tilde{\boldsymbol{\mathcal{F}}}\,, \end{cases} \tag{C.74}$$

where $\hat{\boldsymbol{E}}$ denotes a lift of the Dirichlet data, and the test space $\tilde{\boldsymbol{\mathcal{F}}}$ is a subspace of the "energy space" $\tilde{\boldsymbol{\mathcal{X}}}$ for the stretched variational form (C.74) which can be defined as

$$\tilde{\boldsymbol{\mathcal{F}}} := \{ \boldsymbol{F} \in \tilde{\boldsymbol{\mathcal{X}}} \ : \ \boldsymbol{n} \times \boldsymbol{F} = \boldsymbol{0} \text{ on } \Gamma_D \} \tag{C.75}$$

with

$$\tilde{\boldsymbol{\mathcal{X}}} = \left\{ \boldsymbol{F} \ : \ \frac{|z'|^{\frac{1}{2}}}{|z_i'|} F_i,\ \frac{|z_i'|}{|z'|^{\frac{1}{2}}} (\boldsymbol{\nabla} \times \boldsymbol{F})_i \in L^2(\Omega) \right\}. \tag{C.76}$$

Note that the "energy space" $\tilde{\boldsymbol{\mathcal{X}}}$ is a weighted $\boldsymbol{H}(\text{curl})$ space with weights associated with the derivatives of the stretching functions.

Since the electric and magnetic field redefined according to (C.73) satisfy the original Maxwell's equations in a medium with complex permittivity and permeability constitutive tensors, this form of PML is typically also referred to as *Maxwellian* PML; see e.g. Ref. [30]. With complex permittivity and permeability constitutive tensors redefined according to $\tilde{\epsilon} = \epsilon\tilde{\Lambda}$ and $\tilde{\mu} = \mu\tilde{\Lambda}$ with

$$\tilde{\Lambda} = \mathbf{e}_1\mathbf{e}_1 \left(\frac{z_2' z_3'}{z_1'} \right) + \mathbf{e}_2\mathbf{e}_2 \left(\frac{z_3' z_1'}{z_2'} \right) + \mathbf{e}_3\mathbf{e}_3 \left(\frac{z_1' z_2'}{z_3'} \right), \tag{C.77}$$

such PML formulation yields a physically meaningful material. In contrast, the PML formulation of the linear elasticity equations yields a modified elasticity tensor that is non-physical; cf. Section 3.1.

Bibliography

[1] S. Abarbanel and D. Gottlieb, *A mathematical analysis of the PML method*, J. Comput. Phys. **134** (1997), 357–363.

[2] E. Bécache, P.G. Petropoulos, and S.D. Gedney, *On the long-time behavior of unsplit perfectly matched layers*, IEEE Trans. Antennas Propagat. **52** (2004), no. 5, 1335–1342.

[3] J.-P. Bérenger, *A perfectly matched layer for the absorption of electromagnetic waves*, J. Comput. Phys. **114** (1994), 185–200.

[4] P. Bettess, *Infinite elements*, Penshaw Press, 1992.

[5] J.H. Bramble and J.E. Pasciak, *Analysis of a finite PML approximation for the three dimensional time-harmonic Maxwell and acoustic scattering problems*, Mathematics of Computation, (In press), (2006). Preprint available at : `http://www.math.tamu.edu/~bramble/papers.html`

[6] W.C. Chew, *Waves and fields in inhomogeneous media*, IEEE Press, New York, 1995.

[7] W.C. Chew and J.M. Jin, *Perfectly matched layers in the discretized space: An analysis and optimization*, Electromagnetics **16** (1996), no. 4, 325–340.

[8] W.C. Chew and W.H. Weedon, *A 3D perfectly matched medium from modified Maxwell's equations with stretched coordinates*, Microwave Opt. Techn. Lett. **7** (1994), no. 13, 599–604.

[9] F. Collino and P. Monk, *Optimizing the perfectly matched layer*, Comput. Methods Appl. Mech. Engrg. **164** (1998), 157–171.

[10] L. Demkowicz, *Fully automatic hp-adaptivity for Maxwell's equations*, Comput. Methods Appl. Mech. Engrg. **194** (2005), 605–624.

[11] L. Demkowicz, *Computing with hp-adaptive finite elements. I. One- and two-dimensional elliptic and Maxwell problems*, CRC Press, Taylor and Francis, 2006.

[12] L. Demkowicz and J. Shen, *A few new (?) facts about infinite elements*, Comput. Methods Appl. Mech. Engrg. **195** (2006), 3572–3590.

[13] F.J. Flanigan, *Complex variables: Harmonic and analytic functions*, Dover, New York, 1983.

[14] D. Givoli, *Numerical methods for problems in infinite domains*, Elsevier, Amsterdam, 1992.

[15] M.J. Grote and J.B. Keller, *Exact nonreflecting boundary condition for elastic waves*, SIAM J. Appl. Math. **60** (2000), no. 3, 803–819.

[16] M.N. Guddati and J.L. Tassoulas, *Continued-fraction absorbing boundary conditions for the wave equation*, J. Comput. Acoust. **8** (2000), 139–156.

[17] T. Hagstrom, *New results on absorbing layers and radiation boundary conditions*, Topics in Computational Wave Propagation - Direct and Inverse Problems, Vol. 31 of Lecture Notes in Computational Science and Engineering (M. Ainsworth et al., ed.), Springer, 2003, pp. 1–42.

[18] I. Harari, M. Slavutin, and E. Turkel, *Analytical and numerical studies of a finite element PML for the Helmholtz equation*, J. Comput. Acoustics **8** (2000), no. 1, 121–137.

[19] J.S. Hesthaven, *On the analysis and construction of perfectly matched layers for the linearized Euler equations*, J. Comput. Phys. **142** (1998), 129–147.

[20] F. Ihlenburg, *Finite element analysis of acoustic scattering*, Springer, New York, 1998.

[21] M.C. Junger and D. Feit, *Sound, structures, and their interaction*, The MIT Press, Cambridge, Massachusetts, 1986, 2nd edition.

[22] J. Kurtz and L. Demkowicz, *A fully automatic hp-adaptivity for elliptic PDEs in three dimensions*, (Submitted to Comput. Methods Appl. Mech. Engrg.), (2006).

[23] Q-H. Liu, E. Schoen, F. Daube, C. Randall, and P. Lee, *A three-dimensional finite difference simulation of sonic logging*, J. Acoust. Soc. Am. **100** (1996), no. 1, 72–79.

[24] Q-H. Liu and J. Tao, *The perfectly matched layer for acoustic waves in absorptive media*, J. Acoust. Soc. Am. **102** (1997), no. 4, 1997–2082.

[25] Q.H. Liu, *Perfectly matched layers for elastic waves in cylindrical and spherical coordinates*, J. Acoust. Soc. Am. **105** (1999), no. 4, 2075–2084.

[26] F. Magoulès and I. Harari (eds.), *Special issue on Absorbing Boundary Conditions*, Comput. Methods Appl. Mech. Engrg. **195** (2006), 3551–3902.

[27] P.G. Petropolous, *On the termination of the perfectly matched layer with local absorbing boundary conditions*, J. Comput. Phys. **143** (1998), 665–673.

[28] P.G. Petropoulos, *An analytical study of the discrete perfectly matched layer for the time-domain Maxwell equations in cylindrical coordinates*, IEEE Trans. Antennas Propagat. **51** (2003), no. 7, 1671–1675.

[29] F.L. Teixeira and W.C. Chew, *On causality and dynamic stability of perfectly matched layers for FDTD simulations*, IEEE Trans. Microwave Theory and Techniques **47** (1999), no. 6, 775–785.

[30] F.L. Teixeira and W.C. Chew, *Advances in the theory of perfectly matched layers*, chapter 7 in: Fast and Efficient Algorithms in Computational Electromagnetics (W.C. Chew et al., eds.), Artech House, Boston, 2001, pp. 283–346.

[31] S.V. Tsynkov, *Numerical solution of problems on unbounded domains. A review*, Appl. Num. Math. **27** (1998), 465–532.

[32] Y.Q. Zeng, J.Q. He, and Q.H. Liu, *The application of the perfectly matched layer in numerical modeling of wave propagation in poroelastic media*, Geophysics **66** (2001), no. 4, 1258–1266.